ACS OMEGA

http://pubs.acs.org/journal/acsodf

Article

Effects of Acetylene Addition to the Fuel Stream on Soot Formation and Flame Properties in an Axisymmetric Laminar Coflow Ethylene/Air Diffusion Flame

Xinrong Xie, Shu Zheng,* Ran Sui, Zixue Luo, Shi Liu, and Jean-Louis Consalvi

Cite This: *ACS Omega* 2021, 6, 10371−10382

Read Online

ACCESS | Metrics & More | Article Recommendations

ABSTRACT: The effects of adding acetylene to the fuel stream on soot formation and flame properties were investigated numerically in a laminar axisymmetric coflow ethylene/air diffusion flame using the open-source flame code Co-Flame in conjunction with an elementary gas-phase chemistry scheme and detailed transport and thermodynamic database. Radiation heat transfer of the radiating gases (H_2O, C_2H_2, CO, and CO_2) and soot was calculated using a statistical narrow-band correlated-*k*-based wide band model coupled with the discrete-ordinates method. The soot formation was described by the consecutive steps of soot nucleation, surface growth of soot particles via polycyclic aromatic hydrocarbons (PAHs)-soot condensation or the hydrogen abstraction acetylene addition (HACA) mechanism, and soot oxidation. The added acetylene affected the flame structure and soot concentration through not only chemical reactions among different species but also radiation effects. The chemical effect due to the added acetylene had a significant impact on soot formation. Specifically, it was confirmed that the addition of 10% acetylene caused an increase in the peak soot volumetric fraction (SVF) by 14.9% and the peak particle number density by about 21.1% (z = 1.5 cm). Furthermore, increasing acetylene concentration led to higher concentrations of propargyl, benzene, and PAHs and consequently directly enhanced soot nucleation rates. In addition, the increased H mole fractions also accentuated the soot surface growth. In contrast, the radiation effect of the addition of 10% acetylene was much weaker, resulting in slightly lower flame temperature and SVF, which in turn reduced the radiant heat loss.

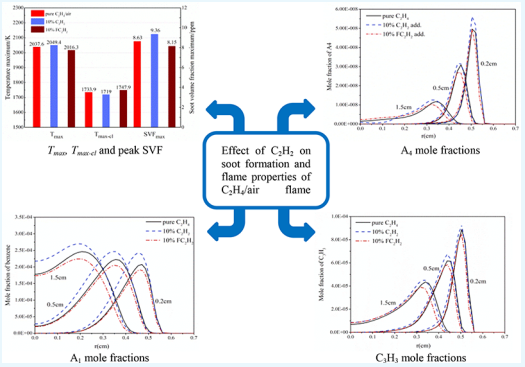

1. INTRODUCTION

Soot is a major undesired product in hydrocarbon combustion due to its adverse effects on energy efficiency, air pollution, and global warming.[1] Adding inert or active additives to the primary hydrocarbon fuel can alter the sooting characteristics of fuel.[2] It is hence essential to understand the soot formation and explore the effect of different additives in fuel. The fuel additives have been paid more and more attention in the past few years, as shown by the study of Kohse-Höinghaus et al.,[3] when reviewing biofuel combustion chemistry. Acetylene has been recognized as the main soot precursor and important combustion intermediate species in hydrocarbon flames;[4] it is necessary to study the effect of acetylene addition to the fuel on combustion.

Recently, He et al.[5] studied the effect of adding N_2 on soot formation in laminar methane, ethane, and propane diffusion flames. The results showed that the addition of N_2 can inhibit the formation of soot through the dilution of the fuel concentration and changing the flame temperature. Zhang et al.[6] pointed out that CO_2 addition inhibited soot formation based on the analyses of dilution, thermal, and chemical effects of CO_2 addition. Liu[7] found that C_2H_2 mole fractions in ethanol flames decreased due to the dilution and thermal effects of CO_2 addition, while the H mole fractions decreased due to the chemical effects of CO_2 addition. Liu et al.[8] revealed the chemical effects of adding CO_2 in both fuel and oxidizer streams of a C_2H_4 diffusion coflow flame. It was shown that C_2H_2 concentration was only slightly reduced when CO_2 was added in the fuel stream, while it decreased by about 10% when CO_2 was added in the oxidizer. They further identified the key reaction steps that accounted for such chemical impacts of CO_2 addition as $CO_2 + CH \rightarrow HCO + CO$ and $CO_2 + H \rightarrow CO + OH$.

To unravel the impact of H_2 addition on soot inception and surface growth, many studies have been conducted for

Received: February 9, 2021
Accepted: March 30, 2021
Published: April 8, 2021

ethylene/hydrogen/air diffusion flames. H_2 is an ideal energy resource because no carbon dioxide or soot is produced in hydrogen combustion. Hydrogen addition in hydrocarbon fuels can reduce the soot emission in diffusion flames[9−11] and improve the combustion efficiency[12,13] and chemical activity.[14,15] Specifically, the experimental investigation of Gülder et al.[16] showed that H_2 addition in the fuel stream inhibited soot formation chemically in a C_2H_4/air laminar coflow flame. However, this chemical inhibition effect of H_2 addition did not exist in C_3H_8/air and C_4H_{10}/air flames. The simulations performed by Guo et al.[11] also verified that H_2 addition in a C_2H_4 diffusion flame inhibited soot formation, which was consistent with ref 16. The numerical results further suggested that the inhibiting effect of H_2 addition was caused by the higher concentration of molecular hydrogen in the lower flame region and the decreased H concentration in soot surface growth regions. Liu and Migliorini[17] studied the influence of adding H_2 on soot formation in coflow laminar CH_4 diffusion flames. It showed that the addition of H_2 or He to CH_4/air flames reduced the soot yield. Lin et al.[10] carried out samplings and simulations of soot formation in C_2H_4 and CH_4 flames with H_2 addition and discovered that H_2 had inhibition and promotion effects on soot in C_2H_4/air and CH_4/air flames, respectively.

Suh and Atreya[18] discussed the chemical effect of H_2O dilution in diffusion laminar CH_4 flames by replacing nitrogen in the oxidant stream with argon and H_2O and found that flame temperature, OH radical concentration, and CO_2 concentration increased due to the addition of water vapor, which in turn suppressed CO concentration. However, the chemical pathway of water vapor was not clear. Liu et al.[19] performed detailed numerical simulations of an axisymmetric diffusion laminar C_2H_4 flame with H_2O addition in the oxidizer to explain the chemical, radiative, and oxygen dilution effects of H_2O on soot formation. They confirmed that the primary pathway for the chemical effect of H_2O addition was mainly via the reaction $H + H_2O \rightarrow OH + H_2$. With increased water vapor concentration, H radical concentration decreased, which in turn led to reduced polycyclic aromatic hydrocarbon (PAH) concentrations.

In addition, some studies were focused on the impact of dual additives on flame properties. Gu et al.[20] studied the effect of adding H_2 and CO_2 on soot formation in coflow axisymmetric C_2H_4 diffusion flames. The results showed that H_2 and CO_2 were more effective in inhibiting soot inception and soot surface growth, respectively. Sun et al.[21] reported the effect of simultaneous H_2 and N_2 addition in C_2H_4/air diffusion flames. The results showed that the flame length increased/decreased when only H_2/N_2 was added and significantly decreased when both H_2 and N_2 were added. Furthermore, they also found that the primary particle diameter decreased in the presence of additional H_2 and N_2 in the fuel stream, while the flame temperature was not affected by H_2/N_2 addition. Ren[22] used N_2, CO_2, and H_2O as dilution species to simulate the CH_4 laminar combustion characteristics. The results showed that the adiabatic flame temperature and burning velocity of CH_4 were decreased by the addition of N_2, CO_2, and H_2O, and the effect of the three species decreased with the decrease of the blending ratios. Mahmoud et al.[23] investigated the effects of H_2O and CO_2 addition as well as the coupling of H_2O and CO_2 addition in diffusion ethylene flames. They revealed that the addition of H_2O to fuel was more effective in suppressing soot formation and that of CO_2 to oxidizer was more effective in soot inhibition.

Although the effects of some additives on the fuel stream or oxidizer stream in different flames have been studied, the previous literature was mainly centered on the effects of H_2, H_2O, and CO_2 addition, while information on the effect of the addition of C_2H_2 on the fuel stream is limited. Zelepouga[24] studied experimentally the effect of adding acetylene and PAHs on soot formation in coflowing nonpremixed CH_4/oxygen and CH_4/oxygen-enriched flames. The results showed that the addition of acetylene and PAHs can enhance soot formation in the four reference flames, containing 21, 35, 50, and 100% of oxygen in the oxidizer stream. The increased soot volumetric fraction (SVF) induced by adding acetylene was significantly smaller due to PAH addition. Kunioshi et al.[25] discussed the effect of adding acetylene or benzene on the PAH growth process in a fuel-rich premixed flame by the modified program and found that production rates of pyrene increased due to the addition of acetylene in early positions of the flame; however, the pyrene concentrations were lower with acetylene addition. The effects of the addition of acetylene to fuel on the flame properties have not been reported in the literature. As a soot precursor, it is essential to understand the role of acetylene, an important combustion intermediate species in hydrocarbon flames. To this direction, the primary objective of the present work is to obtain the effects of the addition of acetylene on soot formation at atmospheric pressure, which were numerically studied in an axisymmetric diffusion laminar ethylene flame. This work investigates the flame structure and chemical and radiation effects of acetylene addition to the fuel. In particular, the detailed reaction pathways for the chemical effects of acetylene are identified.

2. NUMERICAL MODELS

The governing equations of mass, energy, momentum, species, and state were discretized in cylindrical coordinate (r, z). The equations have been elaborated in previous studies[11,26] and were shown as follows. It is, however, worth mentioning that the momentum equations contain a gravity term and the energy equation contains a source term of thermal radiation.

Continuity

$$\frac{\partial}{\partial r}(r\rho v) + \frac{\partial}{\partial z}(r\rho u) = 0 \tag{1}$$

Radial momentum

$$\rho v\frac{\partial v}{\partial r} + \rho u\frac{\partial v}{\partial z} = -\frac{\partial p}{\partial r} + \frac{\partial}{\partial z}\left(\mu\frac{\partial v}{\partial z}\right) + \frac{2}{r}\frac{\partial}{\partial r}\left(r\mu\frac{\partial v}{\partial r}\right) - \frac{2}{3}\frac{1}{r}\frac{\partial}{\partial r}\left(\mu\frac{\partial}{\partial r}(rv)\right) - \frac{2}{3}\frac{1}{r}\frac{\partial}{\partial r}\left(r\mu\frac{\partial u}{\partial z}\right) + \frac{\partial}{\partial z}\left(\mu\frac{\partial u}{\partial r}\right) - \frac{2\mu v}{r^2} + \frac{2}{3}\frac{\mu}{r^2}\frac{\partial}{\partial r}(rv) + \frac{2}{3}\frac{\mu}{r}\frac{\partial u}{\partial z} \tag{2}$$

Axial momentum

https://doi.org/10.1021/acsomega.1c00740
ACS Omega 2021, 6, 10371−10382

$$\rho v\frac{\partial u}{\partial r} + \rho u\frac{\partial u}{\partial z} = -\frac{\partial p}{\partial z} + \frac{1}{r}\frac{\partial}{\partial r}\left(r\mu\frac{\partial u}{\partial r}\right) + 2\frac{\partial}{\partial z}\left(\mu\frac{\partial u}{\partial z}\right) - \frac{2}{3}\frac{\partial}{\partial z}\left(\frac{\mu}{r}\frac{\partial}{\partial r}(rv)\right) - \frac{2}{3}\frac{\partial}{\partial z}\left(\mu\frac{\partial u}{\partial z}\right) + \frac{1}{r}\frac{\partial}{\partial r}\left(r\mu\frac{\partial v}{\partial z}\right) + \rho g_z \quad (3)$$

Energy

$$c_p\left(\rho v\frac{\partial T}{\partial r} + \rho u\frac{\partial T}{\partial z}\right) = \frac{1}{r}\frac{\partial}{\partial r}\left(r\lambda\frac{\partial T}{\partial r}\right) + \frac{\partial}{\partial z}\left(\lambda\frac{\partial T}{\partial z}\right) - \sum_{k=1}^{KK+1}\left[\rho c_{pk}Y_k\left(V_{kr}\frac{\partial T}{\partial r} + V_{kz}\frac{\partial T}{\partial z}\right)\right] - \sum_{k=1}^{KK+1} h_k W_k\omega_k + q_r \quad (4)$$

Chemical species

$$\rho v\frac{\partial Y_k}{\partial r} + \rho u\frac{\partial Y_k}{\partial z} = -\frac{1}{r}\frac{\partial}{\partial r}(r\rho Y_k V_{kr}) - \frac{\partial}{\partial z}(\rho Y_k V_{kz}) + W_k\omega_k \qquad k = 1, 2, ..., KK \quad (5)$$

State equation

$$\rho = \frac{p}{RT\sum_{k=1}^{KK} Y_k/W_k} \quad (6)$$

where v and u are the velocities in the radial (r) and axial (z) directions, respectively, T and ρ are the temperature and density of the mixture, λ is the mixture thermal conductivity, W_k is the relative molecular mass of the k-th species, c_p is the specific heat of the mixture under constant pressure, c_{pk} is the specific heat of the k-th gas species under constant pressure, ω_k is the mole production rate of the k-th gas species per unit volume, h_k is the specific enthalpy of the k-th gas species, g_z is the gravitational acceleration in the axial direction, μ is the viscosity of the mixture, Y_k is the mass fraction of the k-th gas species, V_{kr} and V_{kz} are the diffusion velocities of the k-th gas species in the radial and axial directions, and KK is the total gas-phase species number.

2.1. Soot Formation Model. Because the simplified two-equation soot formation model based on acetylene was unable to predict the detailed physical and chemical processes,[27] it was necessary to apply a more detailed model to study the influence of acetylene addition in this work.

The soot nucleation rate was determined using the collision rate of two pyrene (A_4) molecules and also modified the parameter of van der Waals force.[28] The following soot surface growth and oxidation processes were modeled using the HACA mechanism.[29,30] The soot surface growth can also be caused by collisions between PAH and soot particles, which is generally called the PAH-soot condensation mechanism.[31] The soot-PAH condensation efficiency was set at 0.5. For the HACA mechanism, the parameter of reactive soot surface α was set to 0.004 exp(10,800/T).[32] Further details can be found in refs 4, 26, 32, and 33. This soot formation model has been extensively validated and employed in previous studies.[4,32,33]

2.2. Radiation Model. In the radiation model, the absorption coefficients of combustion products in each band were employed in the calculation of the statistical narrow-band correlated-k model,[34−37] including H_2O, C_2H_2, CO, and CO_2. The soot absorption coefficient was $5.5f_v/\lambda$, where λ and f_v are the wavelength and the volume fraction of soot, respectively. The absorption coefficient was obtained by inverting the cumulative distribution function using the four-point Gaussian integration scheme.[34] The radiation transfer equation was calculated by the discrete-ordinates method (DOM).[38] More detailed calculations on the thermal radiation model can be found in refs 34 and 38.

2.3. Chemical Kinetic Mechanism. The reaction kinetic mechanism of C_2H_4 by the extended Appel, Bockhorn, Frenklach (ABF) mechanism[29] was applied, which included 544 chemical reactions and 103 species. The gas-phase reaction mechanism reported by Appel et al.,[29] which contains PAHs up to pyrene (A_4), was used in this study. It should be pointed out that a relatively new reaction mechanism for C_2 hydrocarbons was developed by Slavinskaya and co-workers at Deutsches Zentrum für Luftund Raumfahrt (DLR),[39] which was shown to perform better than the ABF mechanism in the prediction of soot concentration in the centerline region of a laminar coflow ethylene/air diffusion flame at atmospheric pressure. A recent study by Liu et al.[40] showed that the DLR mechanism fails to predict the chemical effects of CO_2 on soot formation suppression in a laminar coflow ethylene/air diffusion flame. Because of the high CO_2 concentration in the C_2H_2 added combustion flame cases, the ABF mechanism was used in the present numerical study. Also, it has been shown in other studies that the coupling of the ABF mechanism and the soot model described above performed reasonably well in the prediction of soot properties in a laminar axisymmetric coflow ethylene/air diffusion flame.[2,33]

3. COMPUTATIONAL METHODS AND TEST CASES

3.1. Geometry of the Computational Domain. The laminar axisymmetric diffusional ethylene flames were discretized in a two-dimensional matrix region of 3.63 cm (r) × 12.20 cm (z) by 98 (r) ×160 (z) control volumes. Nonuniform meshes were applied to increase the resolution without excessively increasing the computational time. Ethylene (fuel) flowed from a tube of inner diameter 10.74 mm and wall thickness 1.03 mm. Air (oxidizer) flowed out of a concentric annular tube (inner diameter = 88.62 mm). The fuel stream velocity was 3.4 cm/s, and oxidizer velocity was 50 cm/s. Outlet temperatures of the air and ethylene streams were both 300 K. The criterion for simulation convergence was set as when the variation of maximum SVF was less than 1×10^{-5} in two consecutive iterations.

3.2. Numerical Scheme. The governing equations were solved using the control volume method. The convection term was solved using the upwind finite difference method, while the diffusion term was solved through the central differencing scheme. To speed up the convergence process, the discretization equations of soot number density, mass fraction, and gas composition were calculated through complete coupling, while those of pressure correction, energy, and momentum were solved by the tri-diagonal matrix algorithm (TDMA) method.

3.3. Test Cases. Seven test cases were considered to compare the different impacts on flame properties when either acetylene or a fictitious species acetylene was added. The fictitious acetylene (FC_2H_2) in the simulations was invented to facilitate comparisons with real acetylene. It had the same

https://doi.org/10.1021/acsomega.1c00740
ACS Omega 2021, 6, 10371−10382

transport and thermodynamic properties as real acetylene but was chemically inert. It was radiating in Cases 4−5 and nonradiating in Cases 6−7.

The volume fraction compositions of the different cases are shown in Table 1. Case 1 represented the baseline condition with the fuel stream composed of pure ethylene. In Cases 2 and 3, 5 and 10% of C_2H_4 in the fuel stream were replaced by C_2H_2, respectively. The differences between Case 1 and Case 2 contain the global effect of acetylene. In Cases 4 and 5, 5 and 10% of the fictitious species FC_2H_2 were added to the fuel instead, respectively. FC_2H_2 was used to exclude the chemical effect from other effects so that the differences between Cases 2 and 4 were completely due to the chemical effect of acetylene addition. In Cases 6 and 7, 5 and 10% of nonradiating FC_2H_2 were added to the fuel stream, respectively, so that the differences between Cases 4 and 6 were only due to the radiation absorption of acetylene.

Table 1. Compositions of the Fuel Stream of the Test Cases

	fuel stream compositions (volume fraction)			remark
case	$\chi_{C_2H_4}$	$\chi_{C_2H_2}$	$\chi_{FC_2H_2}$	
1	1	0	0	pure C_2H_4
2	0.95	0.05	0	C_2H_2 addition
3	0.90	0.10	0	C_2H_2 addition
4	0.95	0	0.05	radiating FC_2H_2 addition
5	0.90	0	0.10	radiating FC_2H_2 addition
6	0.95	0	0.05	nonradiating FC_2H_2 addition
7	0.90	0	0.10	nonradiating FC_2H_2 addition

4. RESULTS AND DISCUSSION

Zhang et al.[33] validated the soot model with the C_2 mechanism in a diffusion C_2H_4 flame, and Gu et al. applied it in ref 20,where experimental results of H_2 and CO_2 addition effects were reproduced successfully. Therefore, it is adequate to assume that the simulation results of acetylene addition to the ethylene/air flames are at least qualitatively reliable.

In the following discussions, the cases with 10% C_2H_2 and FC_2H_2 in the fuel stream will be elaborated, while the cases with 5% C_2H_2 and FC_2H_2 will be only briefly mentioned because the latter will yield qualitatively same but less obvious results.

4.1. Global Effect of Acetylene Addition. Figures 1 and 2 depict the simulated temperature and SVF distributions for the different cases. Temperature distributions and the corresponding peak temperature (T_{max}) for the pure ethylene/air (Case 1) and 10% acetylene addition (Case 3) are compared in Figure 1a,b. T_{max} was 2037.6 K in Case 1, occurring vertically at 1.0 cm ($-z$) above the burner exit and at the radial distance of 0.49 cm. This closely reproduced the literature hyperspectral experimental result in ref 41 (T_{max} = 2074.0 K at r = 0.51 cm and z = 1.01 cm).

As shown in Figure 1a,b, T_{max} increased by 11.8 K when 10% acetylene was added. Furthermore, the peak centerline temperature ($T_{max\text{-}cl}$, along r = 0) decreased when 10% acetylene was added to C_2H_4/air flames, even though T_{max} was increased. The reason was that the soot concentration of the flame increased and the strong radiation absorption of the soot caused the highest temperature on the centerline to decrease. Besides the effect on the peak flame temperature in the annular region low in the flame, the centerline temperatures between about z = 3.5−6.7 cm became higher as acetylene was added to the fuel stream. Moreover, it was found that adding acetylene from 5 to 10% increased the peak soot volume fraction by about 5.4 and 8.5%. The distributions of CO and CO_2 concentration with and without adding 10% C_2H_2 and FC_2H_2 are compared in Figures 4 and 5, respectively. It can be discovered that acetylene addition to fuel enhanced CO concentration in the flame, as shown in Figure 4a,b, and to a

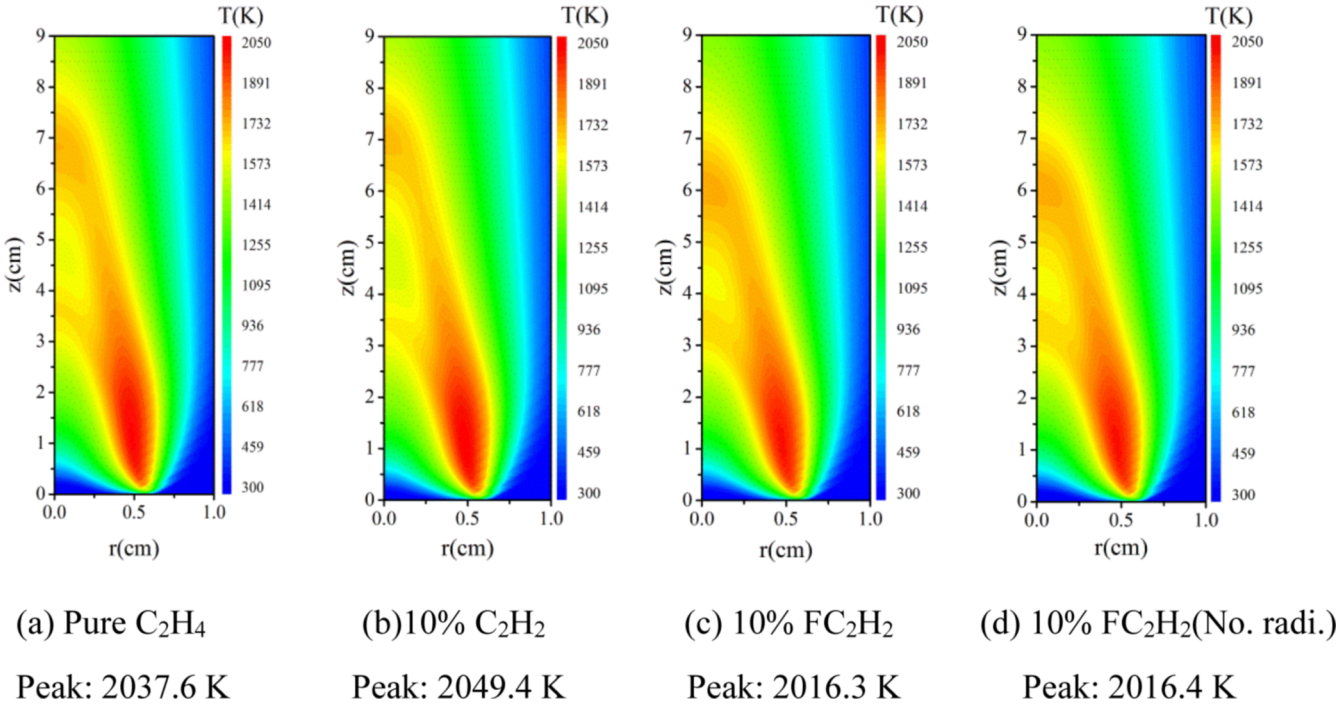

Figure 1. Distributions of temperature in the flames: (a) Case 1, (b) Case 3, (c) Case 5, and (d) Case 7.

https://doi.org/10.1021/acsomega.1c00740
ACS Omega 2021, 6, 10371−10382

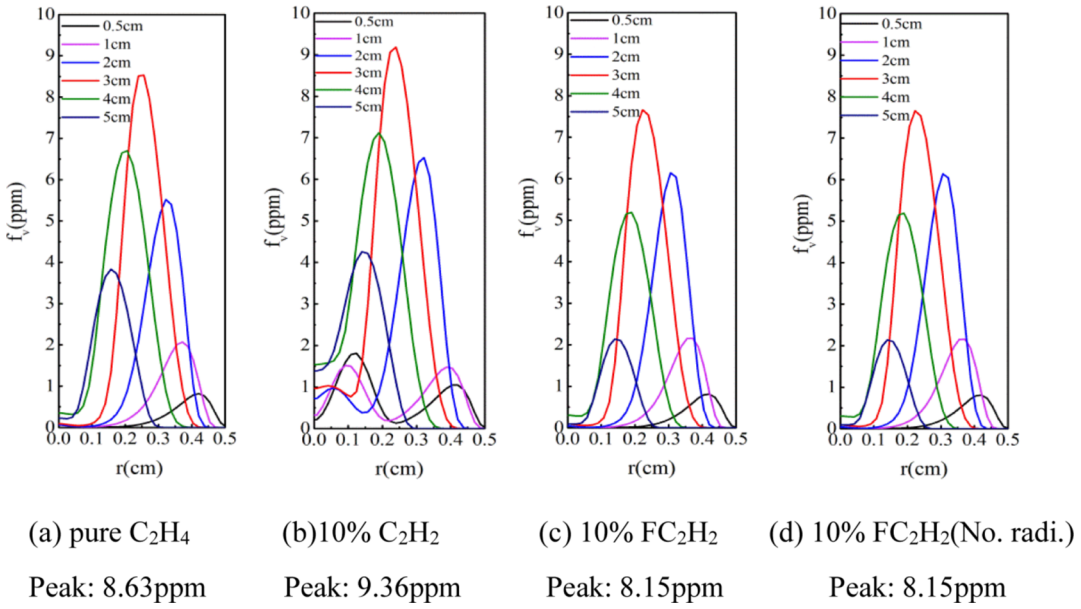

Figure 2. Distribution of SVF in the flames: (a) Case 1, (b) Case 3, (c) Case 5, and (d) Case 7.

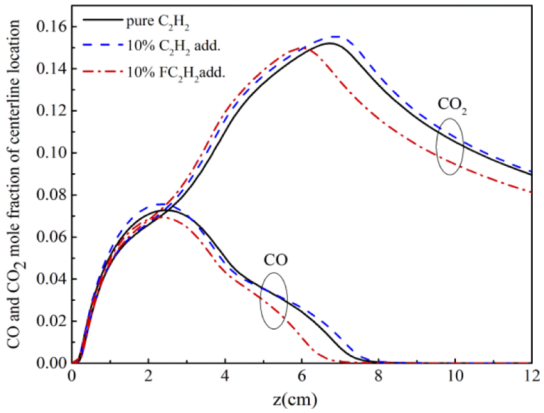

Figure 3. Calculated centerline location distributions of CO and CO_2 concentration of Cases 1, 3, and 5.

lesser extent, enhanced the CO_2 concentration, as shown in Figure 5a,b. The addition of acetylene to ethylene/air fuel also had a slightly global effect on important species such as H_2, H_2O, and so forth, and the maximum mole fractions are shown in Table 2.

4.2. Chemical Effect of Acetylene Addition. To study the chemical effect of C_2H_2 addition, the following discussion will be concentrated on the comparative results of adding 10% C_2H_2 and 10% FC_2H_2. Figure 6 displays the comparisons of T_{max}, $T_{max\text{-}cl}$, and peak SVF in the cases of pure ethylene (Case 1), the addition of 10% C_2H_2 (Case 3), and 10% FC_2H_2 (Case 5). In Case 5, the fictitious species FC_2H_2 had the same transport and thermodynamic properties as C_2H_2, but it was chemically inert. It can hence be used as a "placeholder" of C_2H_2 to exclude other effects but can only the compare chemical effect. It was shown that the chemical effect of the addition of acetylene resulted in an increase of T_{max} by about 1.6% (2016.3 to 2049.4 K when FC_2H_2 and C_2H_2 were added) and led to increased peak SVF by about 14.9%. Moreover, the chemical effect of acetylene caused the $T_{max\text{-}cl}$ to decrease by 1.7%.

Figure 7 depicts the simulated radial profiles of SVF at five vertical positions, 0.14, 0.39, 2.40, 3.30, and 6.09 cm, in flames of pure C_2H_4 (Case 1), 10% C_2H_2 addition (Case 3), and 10% FC_2H_2 addition (Case 5) in the fuel stream. The five heights were selected at the vertical positions where the nucleation rate, PAH-soot condensation rate, surface growth rate through HACA, oxidation rate by OH, and soot oxidation rate by O_2 reached their peaks, respectively.

The chemical effect of 10% C_2H_2 addition is obviously promoting SVF at all five heights. The peak positions of SVF are closer to the centerline at the higher positions during oxidation processes as shown in Figure 7b. SVF was increased by enhancing soot surface growth and mitigating soot oxidation. Two peaks appeared during soot nucleation and PAH condensation processes (at z = 0.14 and 0.39 mm in Figure 7a, respectively), which were caused by the rapid increase of soot inception particles at the upstream regions when C_2H_2 was added. Furthermore, it is observed from Figure 7a that the difference between the red and blue curves at the height of 0.39 cm (only the first peak is considered here) is almost twice that at the height of 0.14 cm. From z = 2.4 cm to 6.09 cm, the discrepancies between the red and blue curves accentuated gradually, although the maximum difference is still lower than that of the first two heights (z = 0.14 and 0.39 cm). It can be concluded that upright along the flame height, the chemical impact of acetylene addition on SVF experienced a nonmonotonic trend, which first increased and then decreased, and finally increased again. These results also indicated that the chemical effect of addition of acetylene is greater on soot nucleation, surface growth by PAH-soot condensation, and HACA mechanism, while the impact on soot oxidation is trivial. The added fictitious acetylene FC_2H_2 did not participate in the chemical reactions and hence was not involved in soot production. In addition, the chemical contribution of O_2 to soot oxidation was greater than that of OH.

Soot nucleation, surface growth by PAH-soot condensation and HACA mechanism, and oxidation are the primary processes influencing SVF. Therefore, it is of considerable significance to explore the dominant chemical pathways of the

https://doi.org/10.1021/acsomega.1c00740
ACS Omega 2021, 6, 10371−10382

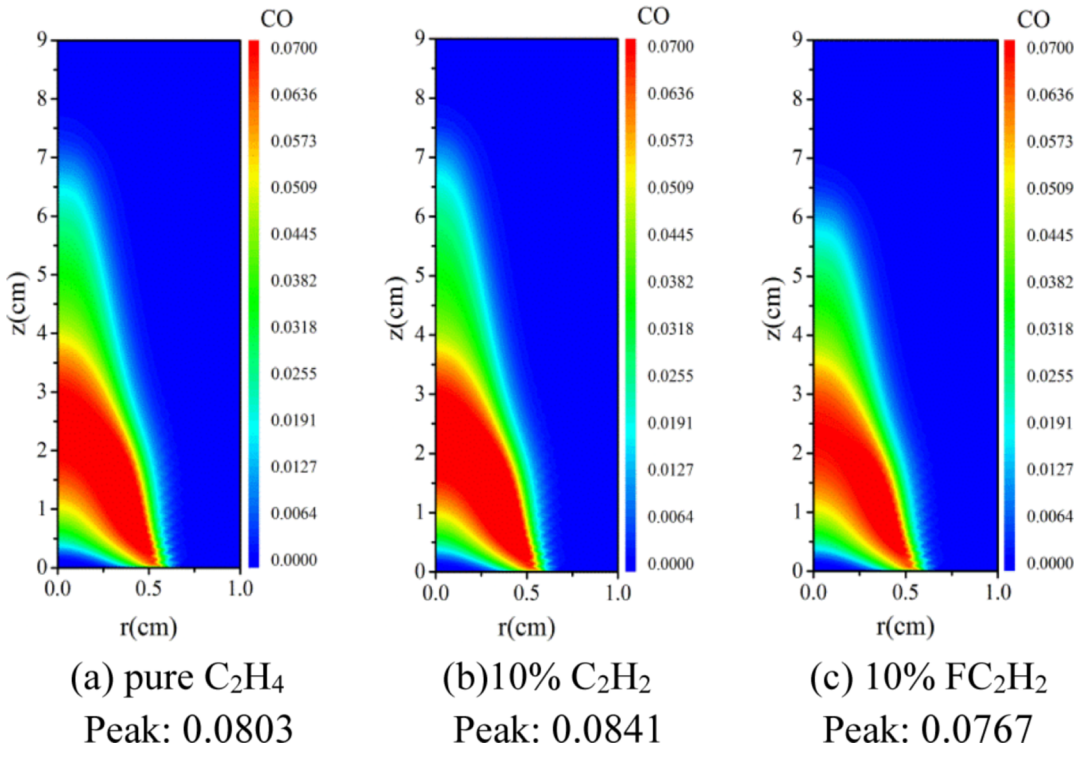

Figure 4. Predicted CO distribution in the flames: (a) Case 1, (b) Case 3, and (c) Case 5.

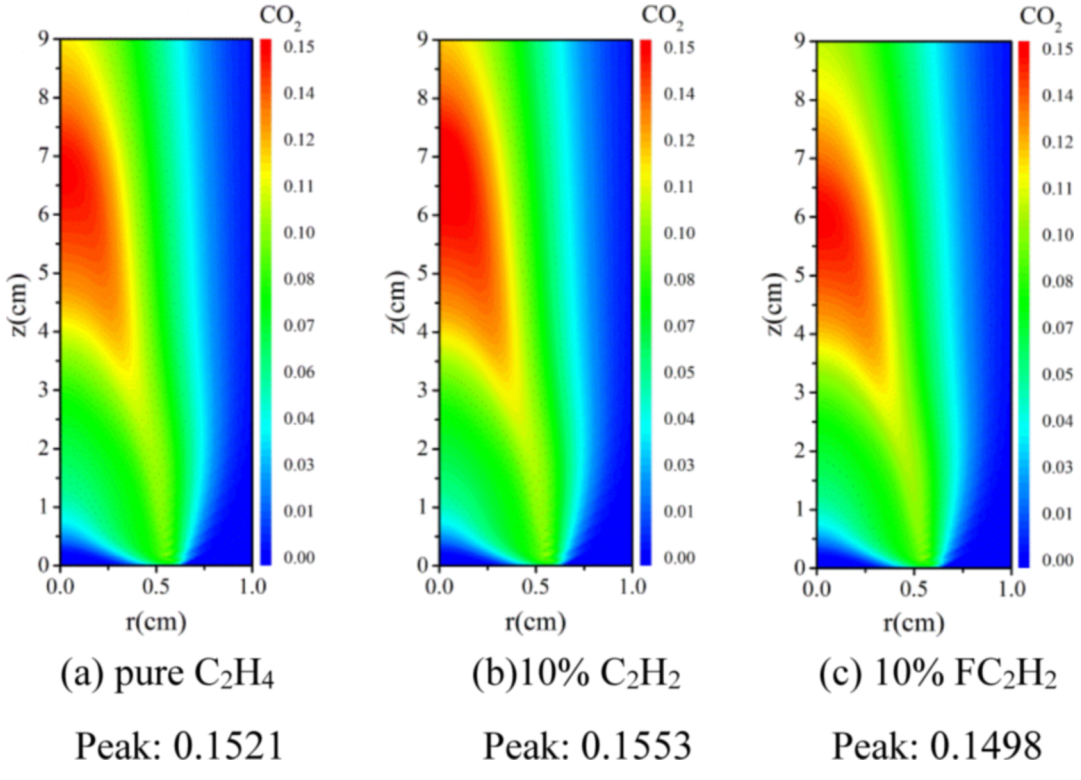

Figure 5. Predicted CO_2 distribution in the flames: (a) Case 1, (b) Case 3, and (c) Case 5.

Table 2. Maximum Mole Fractions of H_2, H_2O, H, and OH

case	$H_{2\text{-max}}$	H_2O_{max}	H_{max}	OH_{max}
pure C_2H_4	4.09×10^{-2}	1.28×10^{-1}	4.37×10^{-3}	5.87×10^{-3}
10% C2H2	4.10×10^{-2}	1.26×10^{-1}	4.39×10^{-3}	5.94×10^{-3}

additional C_2H_2 in C_2H_4/air diffusion flames that influence these processes.

The soot nucleation step is directly controlled by the PAH precursor species, which includes only pyrene (A_4) in the applied formation model of soot. Hence, it is of significance to examine the change of A_4 concentrations due to the additional

https://doi.org/10.1021/acsomega.1c00740
ACS Omega 2021, 6, 10371−10382

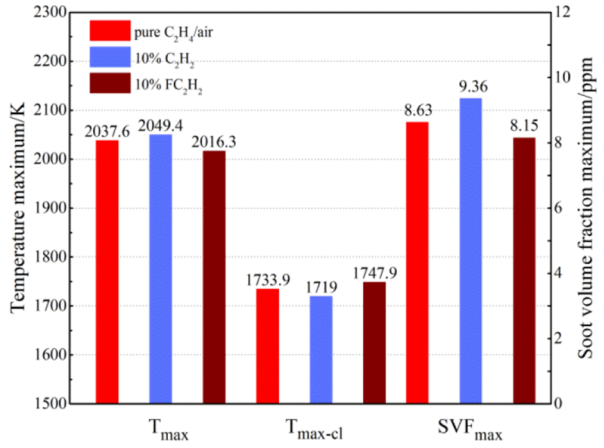

Figure 6. Comparisons of the maximum temperature, the maximum centerline temperature, and the maximum SVF of Cases 1, 3, and 5.

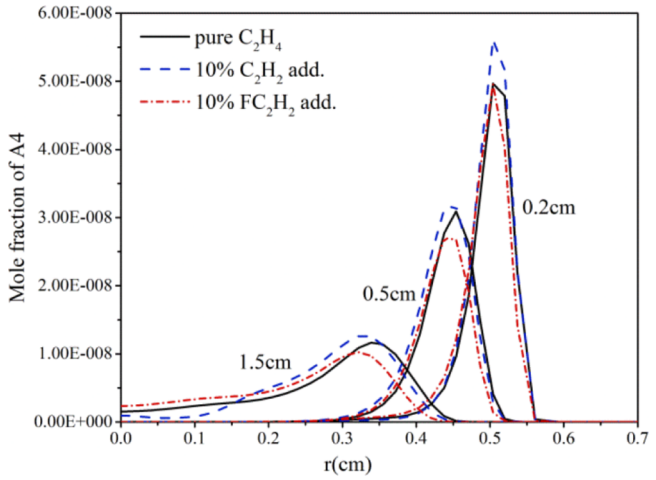

Figure 8. Simulated A_4 mole fractions of Cases 1, 3, and 5 at z = 0.2, 0.5, and 1.5 cm.

acetylene. Figure 8 displays the radial distributions of A_4 concentrations in pure C_2H_4/air flames (Case 1) with 10% C_2H_2 addition (Case 3) and 10% FC_2H_2 addition (Case 5) at the height of 0.2, 0.5, and 1.5 cm. Specifically, the relative increments of maximum A_4 mole fractions are 13.3, 17.8, and 23.5% at the three different heights, respectively. The chemical actions of acetylene increased the A_4 concentration in the annular area above the burner, resulting in higher nucleation rates of soot. It is certain that the distribution of the soot inception rate is consistent with the change trend of the A_4 concentration. The increased A_4 concentration in the initial period of soot formation indicated that the surface growth condensation rate was also high. Because the first ring structured species in the soot formation model is benzene (A_1), which controls the subsequent larger PAH formation, it is also necessary to study the chemical effect of addition of acetylene on A_1 concentration. The calculated radial profiles of A_1 concentration at the three vertical positions are shown in Figure 9. It is clear that the concentration of A_1 increased along with the radial and flow directions, which is aligned with the A_4 results shown in Figure 8. Considering the bottleneck role of

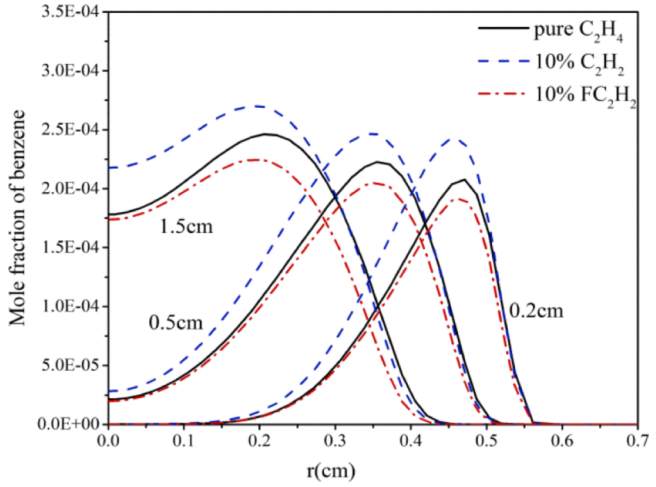

Figure 9. Simulated A_1 mole fractions of Cases 1, 3, and 5 at z = 0.2, 0.5, and 1.5 cm.

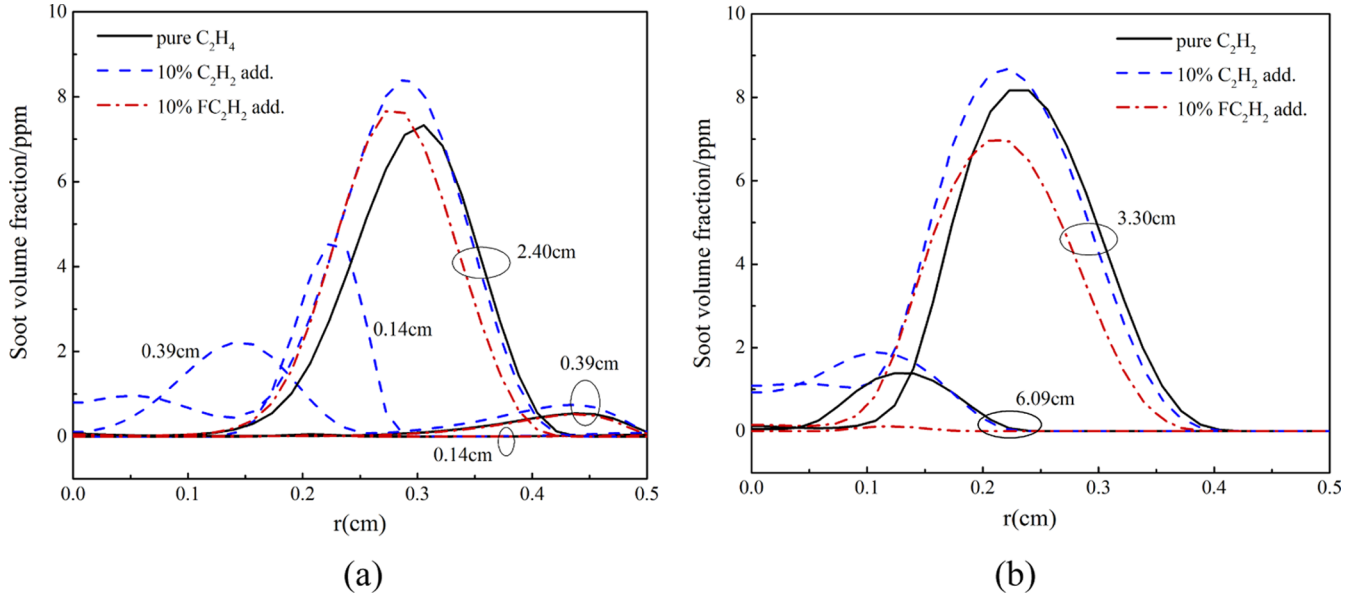

Figure 7. Distributions of SVF at the height of (a) 0.14, 0.39, and 2.40 cm and (b) 3.30 and 6.09 cm of Cases 1, 3, and 5.

https://doi.org/10.1021/acsomega.1c00740
ACS Omega 2021, 6, 10371−10382

A_1 in the formation process of PAHs, it is necessary to analyze in detail the reaction pathway of A_1. As stated in refs 4, 19, 34, and 42 the production steps of A_1 are

$$C_3H_3 + C_3H_3 \leftrightarrow A_1(R234) \quad (7)$$

$$n\text{-}C_4H_5 + C_2H_2 \leftrightarrow A_1 + H(R296) \quad (8)$$

$$1\text{-}C_6H_6 + H \leftrightarrow A_1 + H(R348) \quad (9)$$

$$n\text{-}C_6H_7 \leftrightarrow A_1 + H(R354) \quad (10)$$

Among them, the self-combination step of C_3H_3 is the primary pathway of A_1 formation in C_2H_4/air flames.[4] The simulated C_3H_3 mole fractions at the three heights are shown in Figure 10, where the relative increments of peak C_3H_3 mole

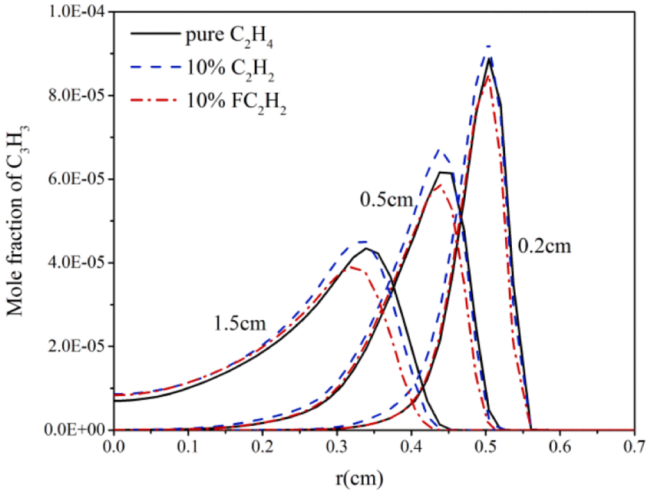

Figure 10. Simulated C_3H_3 mole fractions of Cases 1, 3, and 5 at z = 0.2, 0.5, and 1.5 cm.

fraction are 9.1% (0.2 cm), 14.2% (0.5 cm), and 14.1% (1.5 cm). Obviously, the presence of additional C_2H_2 chemically promoted the C_3H_3 concentration at all positions. Furthermore, acetylene had a stronger chemical effect at higher positions and the peak position moved toward the centerline position.

Next, it is also important to investigate the resulting difference of C_3H_3 mole fractions to further reveal how the chemical effect of acetylene promoted soot formation. C_3H_3 is produced largely via reactions of CH_2 and CH* 2 with acetylene. The combination reactions are as follows

$$C_2H_2 + CH_2 \leftrightarrow C_3H_3 + H(R193) \quad (11)$$

$$C_2H_2 + CH^*2 \leftrightarrow C_3H_3 + H(R194) \quad (12)$$

By examining the reaction rates,[4,19] it was confirmed that the abovementioned two reactions account for approximately 90% of C_3H_3 production in ethylene/air diffusion flames. Consequently, C_3H_3 concentrations were promoted in the presence of additional C_2H_2 (see Figure 10). The increased reaction rates of R193 and R194 were due to the higher C_2H_2 mole fractions (see the radial distributions of acetylene in Figure 11). Moreover, radial distributions of CH_2 concentrations at the three vertical positions of Cases 1, 3, and 5 are shown in Figure 12. Specifically, the relative increment of the CH_2 concentration at the height of 1.5 cm as shown in Figure 12, due to the chemical effect of addition of acetylene, reached

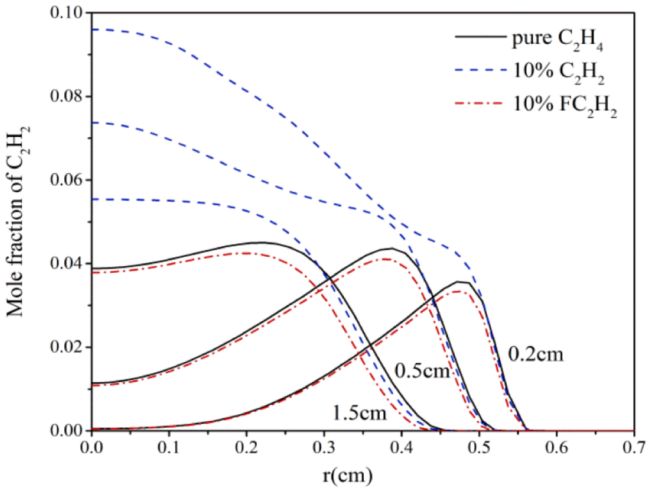

Figure 11. Simulated C_2H_2 mole fractions of Cases 1, 3, and 5 at z = 0.2, 0.5, and 1.5 cm.

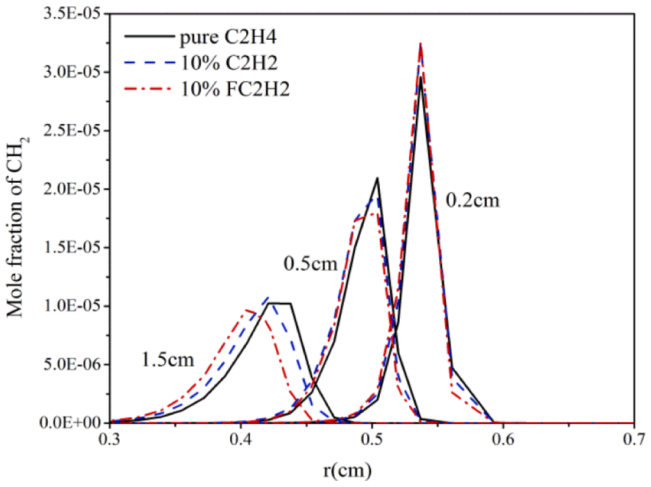

Figure 12. Simulated CH_2 mole fractions of Cases 1, 3, and 5 at z = 0.2, 0.5, and 1.5 cm.

9.9%. It was identified that CH_2 was produced primarily through[19]

$$R146(C_2H_2 + O \leftrightarrow CH_2 + CO) \quad (13)$$

The addition of acetylene in the fuel stream significantly increased the C_2H_2 concentrations at the three vertical positions in the flames, as shown in Figure 11, which consequently formed more CH_2 via R146.

It was also noticed that the presence of additional acetylene significantly increased the peak CO mole fraction and also enhanced the peak CO_2 mole fraction to a smaller extent. For instance, 10% C_2H_2 addition caused an increase of 9.6% in the maximum CO concentration (see Figure 4b,c) but only about 3.7% in the maximum CO_2 concentration (see Figure 5b,c). It can also be observed from Figures 4 and 5 that acetylene addition increased the concentrations of CO and CO_2 along the symmetric centerline. The increment of CO_2 concentration was mainly via

$$CO + OH \leftrightarrow CO_2 + H(R31) \quad (14)$$

and that of CO was primarily via

$$C_2H_2 + O \leftrightarrow CH_2 + CO(R146) \quad (15)$$

https://doi.org/10.1021/acsomega.1c00740
ACS Omega 2021, 6, 10371−10382

Because C_2H_2 is considered to be the only species that promotes soot growth via the HACA mechanism,[4] it is necessary to further explore the reaction pathways of C_2H_2 formation. The chemical effect of adding acetylene to the fuel caused a sharp increase in acetylene concentration in the vicinity of the centerline and until the peak position of acetylene concentration, which remained basically unchanged at the edge of the burner. It is well accepted that C_2H_2 is primarily produced via thermal decomposition of C_2H_4 and the reactions of C_2H_3 with OH and H

$$C_2H_4 \leftrightarrow C_2H_2 + H_2(R164) \quad (16)$$

$$C_2H_3 + OH \leftrightarrow C_2H_2 + H_2O(R160) \quad (17)$$

$$C_2H_3 + H \leftrightarrow C_2H_2 + H_2(R158) \quad (18)$$

The majority of C_2H_3 was created from C_2H_4 via the step $C_2H_4 + H \leftrightarrow C_2H_3 + H_2$ (R166) (19). The radial profiles of C_2H_3 at three vertical positions are shown in Figure 13.

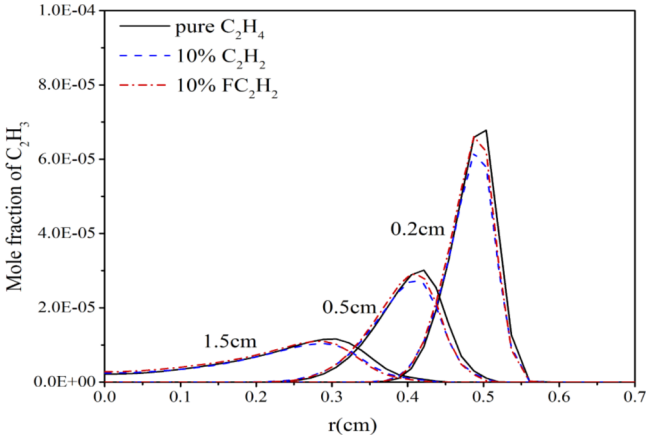

Figure 13. Simulated C_2H_3 mole fractions of Cases 1, 3, and 5 at z = 0.2, 0.5, and 1.5 cm.

It is evident from the abovementioned analysis that C_2H_2 addition in the C_2H_4 fuel stream chemically enhanced the nucleation rates and also influenced the surface growth rates. The surface growth processes included H-abstraction reactions and C_2H_2 addition reactions to form active sites. The key reactions $C_{soot*} + C_2H_2 \rightarrow C_{soot\text{-}H} + H$ (20) and $C_{soot\text{-}H} + H \leftrightarrow C_{soot*} + H_2$ (21) were hence promoted according to the HACA mechanism. As pointed out in refs 29 and 43 the rate of acetylene addition is determined by the HACA mechanism. The forward (positive) reaction rate of H-abstraction is much higher than that of the reverse reaction. Thus, the increased H concentration (see Figure 14) via $C_2H_2 + O \leftrightarrow HCCO + H$ (R144) (22) facilitated the production of more active sites, which in turn led to higher surface growth rates of soot.

Figure 15 shows the reaction rate of soot surface growth R_2 for the Cases of C_2H_4/air flame (Case 1), 10% C_2H_2 (Case 3), and 10% FC_2H_2 in the fuel stream (Case 5). The enhanced 10% maximum surface growth rate was attributed to the chemical effect of acetylene. As reported in ref 44, the surface growth rate of soot is the product of soot surface area per unit volume (A_S) and the specific surface growth rate of soot. Figures 16 and 17 provide the predicted distributions of these quantities at the vertical positions of 0.2, 0.5, and 1.5 cm in Cases 1, 3, and 5. It was found that the A_S increased, while the

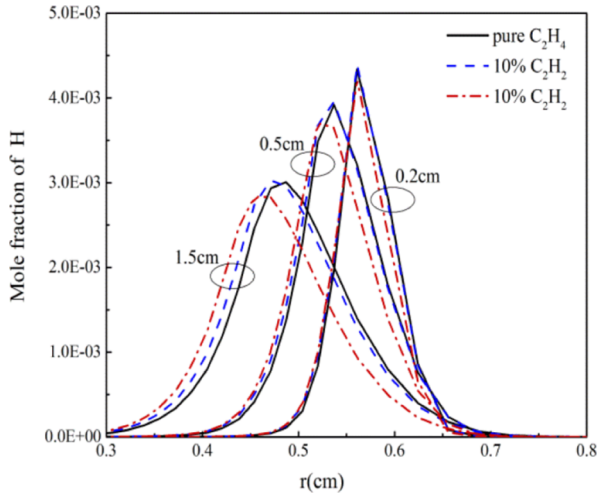

Figure 14. Simulated H mole fractions of Cases 1, 3, and 5 at z = 0.2, 0.5, and 1.5 cm.

specific surface growth rate of soot showed the opposite due to the C_2H_2 addition, which means that the increased A_S, not the specific surface growth rate of soot, caused the higher R_2. It was also found that the difference of A_S was larger than that of the specific surface growth rate of soot (between the blue and red curves), indicating that the chemical effect of acetylene on the larger surface growth rate was caused by the higher A_S.

Figure 18 depicts the calculated number density of soot particles at the same three heights. The specific surface area is equal to the product of the number density and the particle size.

The particle size was determined by the specific surface growth rate of the soot, while the number density was controlled by the nucleation rate. As shown in Figures 17 and 18, the chemical effect of acetylene decreased the surface growth rate by about 2.6% (at z = 1.5 cm), while the particle number density increased by about 21.1% (at z = 1.5 cm), manifesting that the larger number density of the soot particle was dominated by the higher nucleation rate.

4.3. Radiative Effect of Acetylene Addition. The radiative effect[45,46] of acetylene addition to the fuel was "frozen" via the use of the fictitious on-radiating FC_2H_2 in Case 7 for comparison with Case 5 (of radiating FC_2H_2). In both cases, the chemical effects of C_2H_2 were excluded. Figures 2c,d and 3c,d depict the 2D distributions of temperature and SVF, respectively. With 10% acetylene addition, the temperature decreased about 1 K and the SVF decreased only 0.01 ppm due to the radiative effect at the same position. To further amplify the radiation effect of adding acetylene on the flame properties, 40% C_2H_2 and 40% FC_2H_2 with nonradiation acetylene were added to the fuel streams.

5. CONCLUSIONS

A numerical simulation was performed to investigate the effects of acetylene addition in the fuel stream on soot formation in an atmospheric-pressure laminar C_2H_4/air diffusion flame using the open-source code Co-Flame. A soot model based on nucleation by PAH collision, surface growth by PAH-soot condensation or HACA mechanisms, and oxidation reaction was used in conjunction with a detailed C_2 gas-phase chemistry model. The chemical effect of C_2H_2 addition in the fuel stream was "isolated" from other effects by

https://doi.org/10.1021/acsomega.1c00740
ACS Omega 2021, 6, 10371−10382

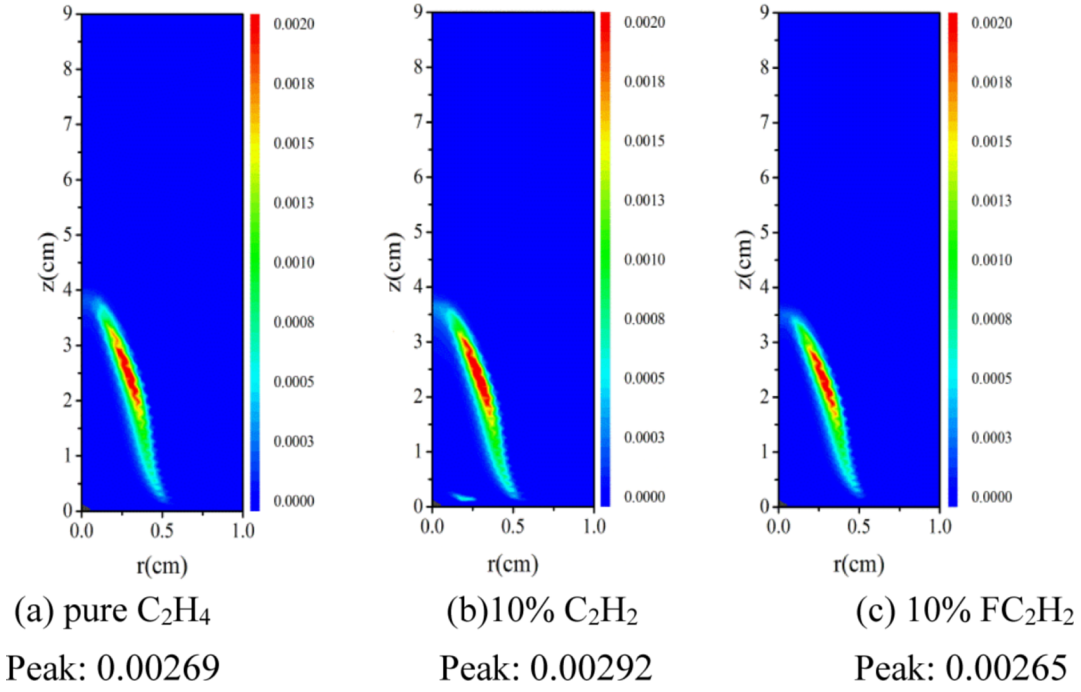

Figure 15. Predicted R_2 distribution in the flames: (a) Case 1, (b) Case 3, and (c) Case 5.

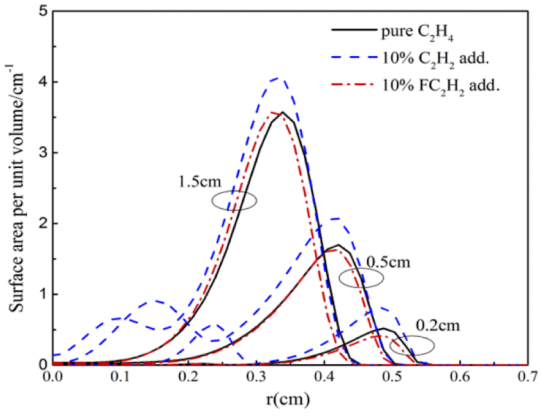

Figure 16. Predicted radial profiles of A_S in the flames of Cases 1, 3, and 5 at vertical positions 0.2, 0.5, and 1.5 cm.

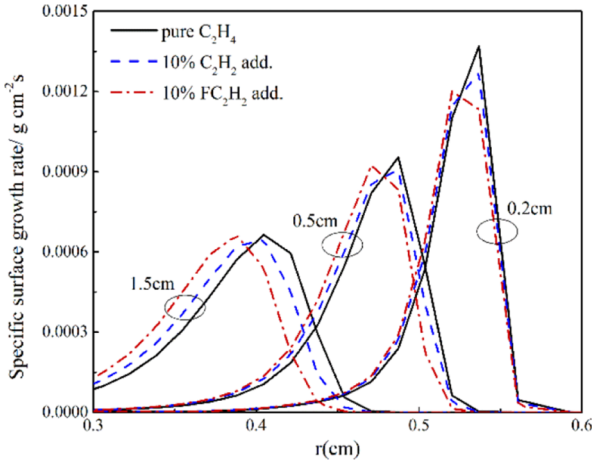

Figure 17. Predicted radial profiles of soot-specific surface growth rate of Cases 1, 3, and 5 at vertical positions 0.2, 0.5, and 1.5 cm.

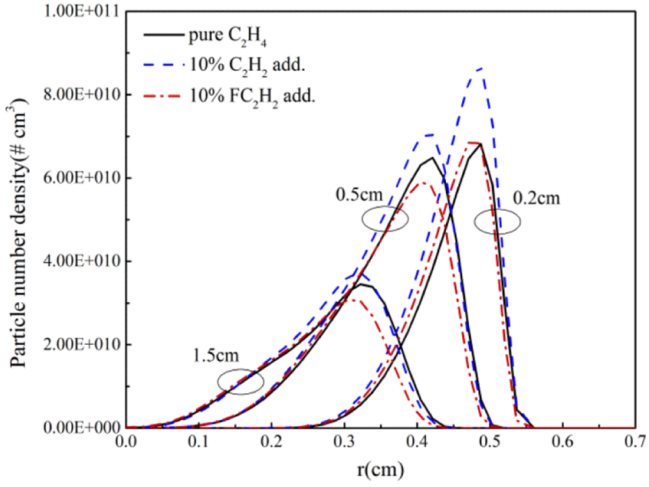

Figure 18. Predicted radial profiles of the particle number density of Cases 1, 3, and 5 at vertical positions 0.2, 0.5, and 1.5 cm.

introducing FC_2H_2 inert species to the chemical reaction mechanism using seven cases of numerical simulation. The present results revealed that 10% acetylene addition in the fuel stream increased the peak flame temperature by 11.8 K and the peak SVF by 8.5%. It was observed that 10% acetylene addition had strong chemical effects, while on the contrary, it had weak radiative effects on the flames. The main reaction pathways of acetylene were obtained through the steps of $C_2H_4 \leftrightarrow C_2H_2 + H_2$, $C_2H_3 + H \leftrightarrow C_2H_2 + H_2$, and $C_2H_3 + OH \leftrightarrow C_2H_2 + H_2O$. Numerical results showed that the chemical effect of 10% acetylene caused the peak flame temperature to increase by 33 K and the peak SVF by 14.9% but caused the peak centerline temperature to reduce by 1.7%. The added acetylene chemically enhanced the concentrations of A_4, A_1, and C_3H_3 in the early period of soot formation. In addition, the chemical effect of acetylene resulted in higher particle number density,

https://doi.org/10.1021/acsomega.1c00740
ACS Omega 2021, 6, 10371−10382

soot specific surface growth rate, and A_S, leading to increased soot inception and surface growth rates.

AUTHOR INFORMATION

Corresponding Author

Shu Zheng − *School of Energy, Power and Mechanical Engineering, North China Electric Power University, Beijing 102206, China;* orcid.org/0000-0002-6107-8931; Email: shuzheng@ncepu.edu.cn

Authors

Xinrong Xie − *School of Energy, Power and Mechanical Engineering, North China Electric Power University, Beijing 102206, China*

Ran Sui − *Department of Mechanical and Aerospace Engineering, Missouri University of Science and Technology, Rolla 65409, Missouri, USA;* orcid.org/0000-0003-3758-7506

Zixue Luo − *State Key Laboratory of Coal Combustion, Huazhong University of Science and Technology, Wuhan 430074, Hubei, China*

Shi Liu − *School of Control and Computer Engineering, North China Electric Power University, Beijing 102206, China*

Jean-Louis Consalvi − *Aix-Marseille Université, IUSTI/UMR CNRS 7343, Marseille Cedex 13 13453, France*

Complete contact information is available at: https://pubs.acs.org/10.1021/acsomega.1c00740

Notes

The authors declare no competing financial interest.

ACKNOWLEDGMENTS

S.Z. was supported by the National Key Research Development Program of China (no.2017YFB0601900), the National Natural Science Foundation of China (nos. 51976057, 51922040, and 51827808), the Fundamental Research Funds for the Central Universities (nos. 2020JG005 and 2019QN014), and the Foundation of State Key Laboratory of Coal Combustion (no. FSKLCCA2104).

REFERENCES

(1) Bond, T. C.; Doherty, S. J.; Fahey, D. W.; Forster, P. M.; Berntsen, T.; DeAngelo, B. J.; Flanner, M. G.; Ghan, S.; Kärcher, B.; Koch, D.; et al. Bounding the role of black carbon in the climate system: A scientific assessment. *J. Geophys. Res.: Atmos.* **2013**, *118*, 5380−5552.

(2) Liu, F.; He, X.; Ma, X.; Zhang, Q.; Thomson, M. J.; Guo, H.; Smallwood, G. J.; Shuai, S.; Wang, J. An experimental and numerical study of the effects of dimethyl ether addition to fuel on polycyclic aromatic hydrocarbon and soot formation in laminar coflow ethylene/air diffusion flames. *Combust. Flame* **2011**, *158*, 547−563.

(3) Kohse-Höinghaus, K.; Oßwald, P.; Cool, T. A.; Kasper, T.; Hansen, N.; Qi, F.; Westbrook, C. K.; Westmoreland, P. R. Biofuel combustion chemistry: From ethanol to biodiesel. *Angew. Chem., Int. Ed.* **2010**, *49*, 3572−3597.

(4) Lorena, M.; Fuster, M.; Millera, A.; Bilbao, R.; Maria U, A. Ethanol as a Fuel Additive: High-Pressure Oxidation of Its Mixtures with Acetylene. *Energy Fuels* **2018**, *32*, 10078−10087.

(5) He, Y.; Qi, S.; Liu, S. Y.; Xin, S. R.; Zhu, Y. Q.; Wang, Z. Y. Effects of the Gas Preheat Temperature and Nitrogen Dilution on Soot Formation in Co-flow Methane, Ethane, and Propane Diffusion Flames. *Energy Fuels* **2020**, DOI: 10.1021/acs.energyfuels.0c03426.

(6) Zhang, C.; Atreya, A.; Lee, K. Sooting structure of methane counterflow diffusion flames with preheated reactants and dilution by products of combustion. *Symp. (Int.) Combust.* **1992**, *24*, 1049−1057.

(7) Liu, D. Chemical Effects of Carbon Dioxide Addition on Dimethyl Ether and Ethanol Flames: A Comparative Study. *Energy Fuels* **2015**, *29*, 3385−3393.

(8) Liu, F.; Guo, H.; Smallwood, G. J.; Gülder, Ö. L. The chemical effects of carbon dioxide as an additive in an ethylene diffusion flame: Implications for soot and NOx formation. *Combust. Flame* **2001**, *125*, 778−787.

(9) Tesner, P. A.; Robinovitch, H. J.; Rafalkes, I. S. The formation of dispersed carbon in hydrocarbon diffusion flames. *Symp. (Int.) Combust.* **1961**, *8*, 801−806.

(10) Lin, Y.; Zhu, B.; Chen, J.; Wu, J.; Lu, K.; Gu, M.; Chu, H. Study of soot functional groups and morphological characteristics in laminar coflow methane and ethylene diffusion flames with hydrogen addition. *Fuel* **2020**, *279*, 118474.

(11) Guo, H.; Liu, F.; Smallwood, G. J.; Gülder, Ö. L. Numerical study on the influence of hydrogen addition on soot formation in a laminar ethylene−air diffusion flame. *Combust. Flame* **2006**, *145*, 324−338.

(12) He, Y. T.; Lian, g M. Q.; Liao, S. Y.; Jian, X. C.; Shao, Y. M.; Jin, Z. Chemical effects of hydrogen addition on low-temperature oxidation of premixed laminar methane/air flames. *Fuel* **2020**, *280*, 118600.

(13) Miao, J.; Leung, C. W.; Huang, Z.; Cheung, C. S.; Yu, H.; Xie, Y. Laminar burning velocities, Markstein lengths, and flame thickness of liquefied petroleum gas with hydrogen enrichment. *Int. J. Hydrogen Energy* **2014**, *39*, 13020−13030.

(14) Hu, G.; Zhang, S.; Li, Q. F.; Pan, X. B.; Liao, S. Y.; Wang, H. Q.; Yang, C.; Wei, S. Experimental investigation on the effects of hydrogen addition on thermal characteristics of methane/air premixed flames. *Fuel* **2014**, *115*, 232−240.

(15) de Ferrières, S.; El Bakali, A.; Gasnot, L.; Montero, M.; Pauwels, J. F. Kinetic effect of hydrogen addition on natural gas premixed flames. *Fuel* **2013**, *106*, 88−97.

(16) Gülder, Ö. L.; Snelling, D. R.; Sawchuk, R. A. Influence of hydrogen addition to fuel on temperature field and soot formation in diffusion flames. *Symp. (Int.) Combust.* **1996**, *26*, 2351−2358.

(17) Liu, F. S.; Migliorini, F.; Cignoli, F.; Iuliis, S. D.; Zizak, G. Effects of hydrogen and helium addition to fuel on soot formation in axisymmetric coflow laminar methane-air diffusion flame. *Asme/jsme Thermal Engineering Heat Transfer Summer Conference Collocated with the Asme Interpack Conference*; American Society of Mechanical Engineers, 2007, No. HT2007-32466.

(18) Justman, S.; Arvind, A. The effect of water vapor on counterflow diffusion flames, In *Proceedings of the International Conference on Fire Research and Engineering*; Peter, D., Angel, E. A., Eds.: Orlando, FL, 1995, September 10-15.

(19) Liu, F.; Consalvi, J.-L.; Fuentes, A. Effects of water vapor addition to the air stream on soot formation and flame properties in a laminar coflow ethylene/air diffusion flame. *Combust. Flame* **2014**, *161*, 1724−1734.

(20) Gu, M.; Chu, H.; Liu, F. Effects of simultaneous hydrogen enrichment and carbon dioxide dilution of fuel on soot formation in an axisymmetric coflow laminar ethylene/air diffusion flame. *Combust. Flame* **2016**, *166*, 216−228.

(21) Sun, Z.; Dally, B.; Nathan, G.; Alwahabi, Z. Effects of hydrogen and nitrogen on soot volume fraction, primary particle diameter and temperature in laminar ethylene/air diffusion flames. *Combust. Flame* **2017**, *175*, 270−282.

(22) Ren, F.; Xiang, L.; Chu, H.; Jiang, H.; Ya, Y. Modeling Study of the Impact of Blending N2, CO2, and H2O on Characteristics of CH4 Laminar Premixed Combustion. *Energy Fuels* **2020**, *34*, 1184−1192.

(23) Mahmoud, N. M.; Yan, F.; Zhou, M.; Xu, L.; Wang, Y. Coupled effects of carbon dioxide and water vapor addition on soot formation in ethylene diffusion flames. *Energy Fuels* **2019**, *33*, 5582−5596.

(24) Zelepouga, S. A.; Saveliev, A. V.; Kennedy, L. A.; Fridman, A. A. Relative effect of acetylene and PAHs addition on soot formation in laminar diffusion flames of methane with oxygen and oxygen-enriched air. *Combust. Flame* **2000**, *122*, 76−89.

(25) Kunioshi, N.; Komori, S.; Fukutani, S. Numerical analysis of the effect of acetylene and benzene addition to low-pressure benzene-rich flat flames on polycyclic aromatic hydrocarbon formation. *Combust. Flame* **2006**, *147*, 1−10.
(26) Zhang, Q. Detailed modeling of soot formation/oxidation in laminar coflow diffusion flames. Ph.D. Thesis, University of Toronto, 2009.
(27) Leung, K. M.; Lindstedt, R. P.; Jones, W. P. A simplified reaction mechanism for soot formation in nonpremixed flames. *Combust. Flame* **1991**, *87*, 289−305.
(28) Frenklach, M.; Wang, H. *Detailed Mechanism and Modeling of Soot Particle Formation*; Springer Berlin Heidelberg, 1994; Vol. *59*; pp 165−192
(29) Appel, J.; Bockhorn, H.; Frenklach, M. Kinetic modeling of soot formation with detailed chemistry and physics: laminar premixed flames of C2 hydrocarbons. *Combust. Flame* **2000**, *121*, 122−136.
(30) Pandey, P.; Pundir, B.; Panigrahi, P. Hydrogen addition to acetylene-air laminar diffusion flames: Studies on soot formation under different flow arrangements. *Combust. Flame* **2007**, *148*, 249−262.
(31) Kronholm, D. F.; Howard, J. B. Analysis of soot surface growth pathways using published plug-flow reactor data with new particle size distribution measurements and published premixed flame data. *Proc. Combust. Inst.* **2000**, *28*, 2555−2561.
(32) Liu, F.; Ai, Y.; Kong, W. Effect of hydrogen and helium addition to fuel on soot formation in an axisymmetric coflow laminar methane/air diffusion flame. *Int. J. Hydrogen Energy* **2014**, *39*, 3936−3946.
(33) Zhang, Q.; Guo, H.; Liu, F.; Smallwood, G. J.; Thomson, M. J. Modeling of soot aggregate formation and size distribution in a laminar ethylene/air coflow diffusion flame with detailed PAH chemistry and an advanced sectional aerosol dynamics model. *Proc. Combust. Inst.* **2009**, *32*, 761−768.
(34) Liu, F.; Smallwood, G. J. An efficient approach for the implementation of the SNB based correlated-k method and its evaluation. *J. Quant. Spectrosc. Radiat. Transfer* **2004**, *84*, 465−475.
(35) Liu, F.; Smallwood, G. J.; Gülder, Ö. L. Application of the statistical narrow-band correlated-k method to low-resolution spectral intensity and radiative heat transfer calculations - effects of the quadrature scheme. *Int. J. Heat Mass Transfer* **2000**, *43*, 3119−3135.
(36) Zheng, S.; Sui, R.; Yang, Y.; Sun, Y.; Zhou, H.; Lu, Q. An improved full-spectrum correlated-k-distribution model for non-gray radiative heat transfer in combustion gas mixtures. *Int. Commun. Heat Mass Transfer* **2020**, *114*, 104566.
(37) Zheng, S.; Sui, R.; Liang, W.; Zhou, H.; Law, C. K. On band lumping, radiation reabsorption, and high-pressure effects in laminar flame propagationflame propagation. *Combust. Flame* **2020**, *221*, 86−93.
(38) Liu, F.; Guo, H.; Smallwood, G. J. Effects of radiation model on the modeling of a laminar coflow methane/air diffusion flame. *Combust. Flame* **2004**, *138*, 136−154.
(39) Dworkin, S. B.; Zhang, Q.; Thomson, M. J.; Slavinskaya, N. A.; Riedel, U. Application of an enhanced PAH growth model to soot formation in a laminar coflow ethylene/air diffusion flame. *Combust. Flame* **2011**, *158*, 1682−1695.
(40) Liu, F.; Karataş, A. E.; Gülder, Ö. L.; Gu, M. Numerical and experimental study of the influence of CO2 and N2 dilution on soot formation in laminar coflow C2H4/air diffusion flames at pressures between 5 and 20 atm. *Combust. Flame* **2015**, *162*, 2231−2247.
(41) Liu, H.; Zheng, S.; Zhou, H. Measurement of soot temperature and volume fraction of axisymmetric ethylene laminar flames using hyperspectral tomography. *IEEE Trans. Instrum. Meas.* **2017**, *66*, 315−324.
(42) Eaves, N. A.; Zhang, Q.; Liu, F.; Guo, H.; Dworkin, S. B.; Thomson, M. J. CoFlame: A refined and validated numerical algorithm for modeling sooting laminar coflow diffusion flames. *Comput. Phys. Commun.* **2016**, *207*, 464−477.
(43) Yang, W.; Parker, T.; Ladouceur, H. D.; Kee, R. J. The interaction of thermal radiation and water mist in fire suppression. *Fire Saf. J.* **2004**, *39*, 41−66.
(44) Guo, H.; Thomson, K. A.; Smallwood, G. J. On the effect of carbon monoxide addition on soot formation in a laminar ethylene/air coflow diffusion flame. *Combust. Flame* **2009**, *156*, 1135−1142.
(45) Wang, F.; Wang, H.; Gong, D.; Cheng, Z.; Ma, L. Radiative transfer analysis of semitransparent medium with particles having non-uniform size distribution by differential-integration method. *Int. Commun. Heat Mass Transfer* **2019**, *130*, 342−355.
(46) Zheng, S.; Yang, Y.; Sui, R.; Lu, Q. Effects of C2H2 and C2H4 radiation on soot formation in ethylene/air diffusion flames. *Appl. Therm. Eng.* **2021**, *183*, 116194.

https://doi.org/10.1021/acsomega.1c00740
ACS Omega 2021, 6, 10371−10382